ADVANCED ENGINEERING MATERIALS
www.aem-journal.com

A Constitutive Stress–Strain Law for Metals with Sigmoidal Curves

Trevor William Clyne and Wenchen Gu*

A formulation is proposed for true stress–true strain relationships in the plastic regime that exhibit sigmoidal shapes, such as those of certain metastable austenitic stainless steels (MASS). It contains two terms, broadly accounting for contributions to hardening from conventional plasticity and from mechanical stimulation of martensite formation. It is a continuous function, designed to cover the plastic strain range from zero up to several tens of percent. It is shown that it is suitable for capture of a range of curve shapes of this type—experimental data from tensile testing of a MASS alloy over a range of temperature, with good fidelity. The formulation incorporates six independent parameters, although there may be scope for limiting the range of values that they can have, facilitating convergence operations. Information is presented about how convergence is obtained. The equation is thus expected to be suitable for use in finite element method (FEM) models for simulation of plastic deformation in various scenarios, including indentation. Future work will involve exploration of the details of this.

1. Background

1.1. Constitutive Laws for Quasistatic Metal Plasticity

The mechanisms of plastic deformation are complex and there is no prospect of being able to predict the stress–strain curves exhibited by metals in any fundamental way. However, there are strong incentives to capture these curves via empirical formulations. These focus on the relationship between true stress and true (plastic) strain. These are the von Mises (deviatoric) components of the stress and strain tensors, which are both scalars. There is a marked tendency for this stress (sometimes termed "flow stress") to increase as the plastic strain increases. However, the "work hardening rate" (gradient of the true stress–strain curve after yielding) can vary over a wide range. Also, the way that the work hardening rate changes (usually reduces) with increasing plastic strain can vary substantially.

Such relationships should ideally be valid over an appreciable range of plastic strain—perhaps 50% or more in some cases. Of course, there is no expectation that the curve will in fact conform perfectly to any particular functional form over such a range. However, in general, the work hardening rate tends to decrease progressively with increasing strain, perhaps eventually approaching zero. This is largely a consequence of competition between the creation of new dislocations and inhibition of their mobility (by forming tangles, etc.) and processes (such as climb and cross-slip) that will allow them to become more organized and annihilate each other. Initially, the former group of processes tends to dominate, but a balance may eventually be reached, such that the flow stress ceases to rise. Cases in which the work hardening rate increases with increasing strain are usually considered to be relatively rare, at least with metallic polycrystals. In fact, a type of metal that does exhibit such behavior has become industrially more significant recently and this is the focus of the current article. However, most constitutive laws relate to cases in which the work hardening rate decreases monotonically with increasing plastic strain.

Several analytical expressions have been proposed, but two are in the most frequent use. The first is the Ludwik–Hollomon equation.[1]

$$\sigma = \sigma_Y + K\varepsilon^n \tag{1}$$

where σ is the (von Mises) applied stress, σ_Y is its value at yield, ε is the plastic (von Mises) strain, K is the "work hardening coefficient," and n is the "work hardening exponent." The second is the Voce equation.[2]

$$\sigma = \sigma_s - (\sigma_s - \sigma_Y)e^{-\varepsilon/\varepsilon_0} \tag{2}$$

The stress σ_s is a "saturation level," whereas ε_0 is a "characteristic strain" for the exponential approach of the stress toward this level. It can be seen that both laws involve three independent parameters, with the plasticity thus being fully captured by a set of three numerical values.

These equations are generally found to be satisfactory for representation of a wide range of experimental stress–strain curves. This is shown in **Figure 1**, which compares [3] experimental data [4] for three different types of stainless steels with best fit plots

T. W. Clyne, W. Gu
Plastometrex Ltd
04 Science Park, Milton Road, Cambridge CB4 0GZ, UK
E-mail: b.clyne@plastometrex.com

T. W. Clyne
Department of Materials Science
University of Cambridge
27 Charles Babbage Road, Cambridge CB3 0FS, UK

The ORCID identification number(s) for the author(s) of this article can be found under https://doi.org/10.1002/adem.202100739.

DOI: 10.1002/adem.202100739

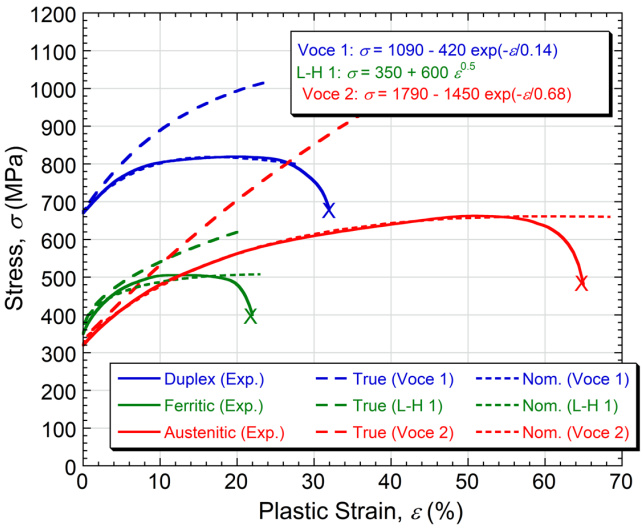

Figure 1. Comparison between experimental tensile test data for three different types of stainless steel, reported as nominal stress–nominal strain plots, and best fit curves obtained using Ludwik–Hollomon or Voce equations (for true stress–true strain relationships). Reproduced with permission.[3] Copyright Cambridge University Press, Cambridge, UK 2021

obtained using Ludwik–Hollomon and Voce expressions. It can be seen that, despite the three experimental (nominal stress–strain) curves having very different shapes, all of them can be captured quite well using these simple analytical equations. Of course, agreement can only be anticipated up to the onset of "necking," which is expected to start at the peak of the nominal stress–nominal strain curve. After that point, the distributions of strain and stress in the sample start to become highly inhomogeneous and their relationship with the plot becomes complex. However, this complexity can in many cases be captured in an FEM model of the test,[3] often using a single true stress–true strain relationship and applying it so as to simulate neck formation and even the final fracture event (based on a critical true strain criterion).

1.2. Metals Exhibiting Sigmoidal Stress–Strain Curves

There are certainly some metallic samples that exhibit stress–strain curves which cannot be captured via formulations of the type described earlier. One example is provided by single crystals, which often show an initial "easy glide" regime with approximately constant stress levels (in which only one slip system is operative), followed by work hardening as further slip systems are activated and dislocations start to interact with each other and become less mobile. Another is materials that show an initial load drop as dislocations escape from their solute "atmospheres," followed by a pulse of straining at constant load while they move, driven by released strain energy. However, in practice, single crystals constitute a rather special class of materials, with their behavior exhibiting a strong dependence on their orientation with respect to the loading axis, whereas few metals of industrial significance actually exhibit a pronounced load drop. The need for constitutive laws to describe the plasticity of metals in which the work hardening rate does not decrease monotonically has therefore been limited.

However, there is a class of metals, of increasing industrial significance, in which the work hardening rate does increase sharply with increasing strain, followed by a decrease. The resulting stress–strain curves are often described as sigmoidal. Among the most prominent of such materials is the class usually referred to as metastable austenitic stainless steels (MASS). The rise in work hardening rate comes in this case from the mechanical stimulation of martensite formation, which often starts to take place only after appreciable plastic deformation of the austenite occurs (with little work hardening). The exact behavior depends on several factors, including the temperature (as the thermodynamic driving force for martensite formation is greater at lower temperature) and the stacking fault energy, with a low value facilitating the cross-slip that can be involved in phase transformation. The composition is important, including the carbon and nitrogen levels. High levels of these tend to retard martensite formation, although very low levels of carbon lead to a reduction in the hardness of the martensite. There is in fact a relatively small "window" of composition and conditions for which the effect is pronounced. However, there is strong interest in promoting such behavior, as it is very favorable in terms of energy absorption and crashworthiness. In fact, usage of steel sheet of this type is increasing markedly in the automotive industry.

A number of papers[5–8] have been published that present both theoretical background relating to the mechanical behavior of MASS and experimental stress–strain curves (converted in some cases to true stress–true strain relationships, using the analytical relationships that apply up to the onset of necking). It is clear that mechanical stimulation of the formation of martensite, with an associated increase in the "hardness" (work hardening rate) can have a marked effect on the nature of the curve. One of the issues involved here is whether the austenite–martensite phase transformation is significantly affected by the hydrostatic component of the stress state, which would manifest as a "tensile-compressive asymmetry" during uniaxial testing. Certainly the fact that transformation is accompanied by a significant volume change (an increase in around 4–5%) might be expected to promote a dependence of some sort. Work in this area has so far been rather limited and inconclusive.[9–13] It is thus not at present clear whether conventional FEM simulation of a generalized stress state, based only on the von Mises values of stress and strain (with no account taken of the hydrostatic component), is expected to be fully reliable; this is an area requiring further work.

In any event, a representative set[7] of tensile stress–strain curves is shown in **Figure 2**, relating to a particular MASS steel tested over a range of temperatures. The changes in work hardening rate, particularly the increase after a plastic strain of the order of 5–10%, are quite dramatic. It is clear that such behavior cannot be captured, even approximately, using existing formulations such as those of Voce and Ludwik–Hollomon.

It may also be noted that there is no information available about the shapes of such curves beyond the true strain levels at which necking occurs during tensile testing. Possibly this could be obtained via compressive testing (if there is in fact no significant asymmetry), but in that case conversion between nominal and true values of stress and strain using the analytical relationships would be inaccurate from the start, due to the effects of friction. It would be possible to conduct iterative FEM modeling of either type of test, so as to infer a true

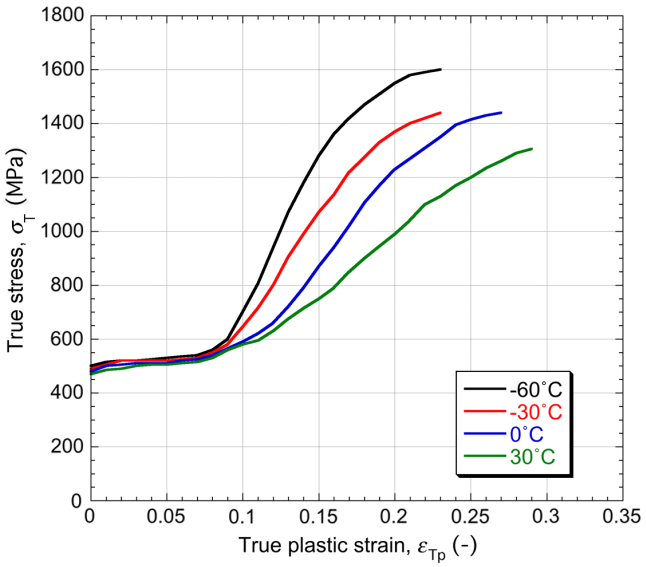

Figure 2. Experimental data[7] for tensile testing of AISI 301LN steel over a range of temperature, converted to true stress–true strain relationships (up to the onset of necking).

stress–true strain relationship from the nominal data, but this requires it to be represented using a functional form—see below. It may finally be noted, however, that, in view of the high work hardening rates over the approximate range of 10–25%, it may be that strain localization is strongly inhibited and the creation of strains well above that range is relatively rare. Of course, this is consistent with the concept of good crashworthiness, as energy absorption will tend to be distributed into large volumes of material surrounding an impact site.

1.3. Iterative FEM Simulation of Plastic Deformation Processes

There is a particular context in which the availability of constitutive laws that capture well the plasticity of different types of metal is essential. This is the iterative FEM simulation of a plasticity test, converging on the set of parameter values giving the best fit between measured and modeled outcomes. This is a well-established procedure and its usage is central to a recently developed testing methodology, termed profilometry-based inverse FEM for indentation plastometry (PIP). Its emergence is the outcome of an extended period of research and development.[14–21] It is based on iterative FEM simulation of the indentation process, with the plasticity parameters (in a constitutive law) being repeatedly changed until optimum agreement is reached between experimental and predicted outcomes. While the outcome that was used in much early work was the load–displacement plot, it has become clear that using the residual indent profile offers major advantages.[21] The superior reliability of PIP to the so-called instrumented indentation technique (IIT) methodology of converting a load–displacement plot to a stress–strain curve via analytic relationships has been clearly demonstrated.[22] PIP has already been successfully applied to several industrial scenarios, including a thin plasma-sprayed layer[23] and (anisotropic) additively manufactured material,[24] both Ni-based superalloys. It has also been confirmed[25] that the presence of residual stresses in a sample is unlikely to have a strong effect on the reliability of extracted stress–strain curves.

Several points concerning optimization of this procedure have recently become clear. One of these[18] is that a spherical indenter is preferable to a "sharp" one. Others include the importance of deforming a volume that is large enough for its mechanical response to be representative of the bulk, which usually requires it to be a "many-grained" assembly. This typically translates into a need for the indenter radius to be of the order of 1 mm and the load capability to extend to the kN range. This means that equipment designed for what is often described as "nanoindention" is completely unsuitable and a customized loading frame is required. In fact, commercial PIP systems incorporate a loading frame, a profilometer, and a software package that allow automated convergence on the best fit true stress–strain curve. Of course, once that has been established, then FEM simulation of any loading configuration, including a uniaxial tensile test, can readily be conducted.

The most current commercial use of PIP is based on the Voce constitutive law. This has been found to be satisfactory for the vast majority of metals. However, it is clear that it would not lead to reliable stress–strain curves for metals exhibiting behavior such as that in Figure 2. It may be noted at this point that both Voce and Ludwik–Hollomon equations have only three independent parameters, so convergence is required in three-parameter space. It seems clear that more parameters than this are needed to capture a sigmoidal curve in a flexible way. Of course, other things being equal, convergence tends to become slower and less efficient as the number of parameters is increased. However, it is perhaps worth mentioning that the operation can be greatly facilitated if the range of possible values of some or all of the parameters is limited, such that a starting point in parameter space can be chosen that is fairly close to the "solution."

2. Development of a Formulation for Sigmoidal Curves

2.1. Previous Proposals

There have been very few attempts to formulate analytical equations for representation of sigmoidal stress–strain curves. Mukarati et al.[26] recently proposed one, but it is based on different expressions for the strain regimes before and after the onset of "martensitic" hardening, and it also involves the strain rate. To conduct iterative FEM simulation of a process (such as indentation), a single expression is required that is applicable across the complete range of plastic strain, preferably up to at least several tens of %.

2.2. Proposed Formulation

A central problem with the sigmoidal shape is that it is difficult to capture with a single functional form. There are certainly functions that asymptote at high strain to a capped level—indeed the Voce equation does this. This is commonly achieved via expressions involving exponential terms. However, single expressions of this type are unlikely to give sufficient freedom to capture well the shape of the sigmoidal part. This limitation, and a possible approach to reducing it, is shown by the curves in **Figure 3**,

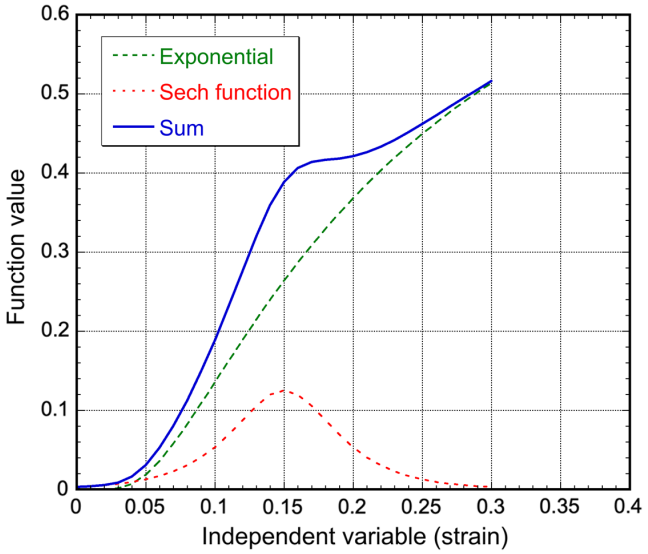

Figure 3. Curves illustrating how a sigmoidal shape can be obtained by summing two functions.

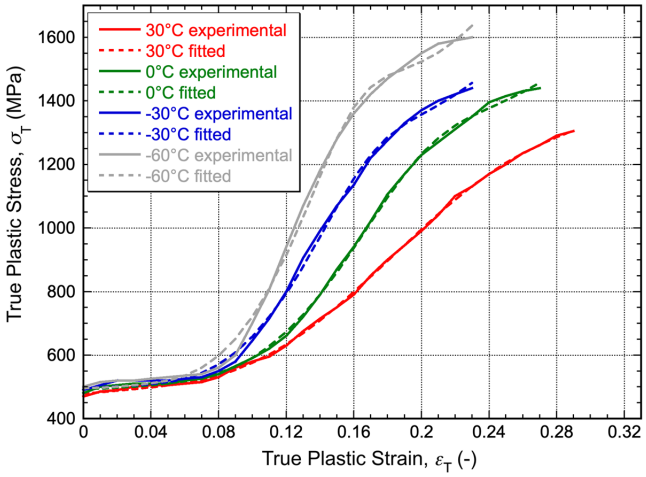

Figure 4. Comparisons between the experimental curves of Figure 2 and corresponding best fit plots of Equation (5), obtained using the sets of parameter values shown in Table 1.

which shows how summing two functions gives greater freedom to tailor the sigmoidal part. While this analogy cannot be taken very far, this could be considered to reflect the fact that two different hardening mechanisms are active in these metals, making contributions over different ranges of strain.

The functions used in constructing Figure 3 are

$$y = e^{-A/x} \tag{3}$$

$$y = \frac{\mathrm{sech}(B(x - C))}{D} \tag{4}$$

The values of A, B, C, and D used to create the curves in the figure were 0.2, 30, 0.15, and 8 respectively. The value of A controls the initial rate of rise of the exponential function and the value of x at which it will start to asymptote (to 1.0). The sech function has a peak at an x value of C, whereas its width and magnitude are respectively controlled by B and D. Of course, the plot is only intended to be illustrative and these parameter values can be varied to give a wide range of net shapes. Clearly the overall expression will also need to include reference stress levels (for the initial yielding and for a level at high strains). A possible formulation is therefore

$$\sigma = \sigma_Y + (\sigma_F - \sigma_Y)\left(e^{-\varepsilon_S/\varepsilon} + \frac{\mathrm{sech}(B(\varepsilon - \varepsilon_M))}{D}\right) \tag{5}$$

where σ_Y is the yield stress, σ_F is the flow stress at high levels of strain, ε_S is a characteristic strain for "standard" plasticity, and ε_M is the strain at which martensite formation makes its peak contribution to hardening.

2.3. Fidelity of Representation

An obvious test of whether Equation (5) is "fit for purpose" is to check whether sets of parameter values can be found that capture with good fidelity experimental curves such as those in Figure 2. A comparison is shown in **Figure 4**. The sets of parameter values used to obtain these functional curves are shown in **Table 1**. Also shown there are the corresponding values of the "misfit parameter," S_{red}, which characterizes the "goodness of fit." Any value below about 10^{-3} represents good fit. (Perfect fit corresponds to a value of zero.) It can be seen that all of these curves fit well with the experimental data.

The convergence operation used to obtain these "best fit" sets of parameter values was the Nelder–Mead simplex algorithm.[27] Details of how this has been implemented, including the definition of S_{red}, are available in the literature.[18] An arbitrary starting point in parameter space was chosen, although the value of each parameter was set within a range that was known to be broadly appropriate. Convergence typically required a few 100 iterations. The corresponding requirement in terms of computational time will obviously depend on several factors, but in general the operation is expected to be tractable.

Table 1. Values of the independent parameters in Equation (5) used in constructing the curves shown in Figure 4.

Plot	Parameter						
	Yield Stress, σ_Y [MPa]	Flow Stress, σ_F [MPa]	Standard Strain, ε_S	Martensitic Strain, ε_M	Martensitic Width, B	Martensitic Magnitude, D	Misfit, S_{red}
−60 °C	489.0	6654.2	0.408	0.161	30.02	15.07	4.6×10^{-4}
−30 °C	491.2	5665.6	0.414	0.170	26.79	18.10	2.1×10^{-4}
0 C	483.1	6045.1	0.515	0.202	20.95	17.05	7.5×10^{-5}
30 °C	450.0	3674.5	0.473	0.239	12.13	11.88	3.4×10^{-5}

Certain points are worthy of note. One issue is whether all six of the parameter values have to be regarded as independent variables. It seems clear that the two stress levels must be independent: as it happens, all of the curves in Figure 2 have similar yield stress levels, but obviously that will not be true for all sigmoidal curves. It does appear that all of the others do vary, although it may be noted that the ranges are relatively narrow for some of them. As mentioned earlier, convergence operations are always more efficient if the ranges of possible values for the independent variables can be constrained within fairly tight limits, irrespective of how many of them have to be considered.

Incidentally, it may be helpful to note the physical significance of the parameter values in Table 1. The significance of the yield and flow stress values is self-evident. The "standard strain" controls the strain level at which conventional hardening starts to become significant, which is somewhat delayed in alloys of these types. The "martensitic strain" is the strain level at which "martensitic hardening" reaches a peak. Finally, the parameters B and D, respectively, control the width (strain range) over which martensitic hardening occurs and its relative significance, compared with "standard" hardening. It may be noted, however, that both of these parameters work inversely, that is, a large value of B gives a narrow strain range and a large value of D corresponds to a low relative significance of martensitic hardening. For example, it can be seen from the values of B in Table 1 that there is a broad trend for martensitic hardening to be concentrated over a narrower range of strain at lower temperatures (due to the higher thermodynamic driving force for its formation, so that less straining is needed to stimulate it). However, as mentioned earlier, any correlation between functional relationships in a constitutive law and actual mechanisms of plastic deformation can only be a loose and qualitative one.

Future work is planned in which PIP testing is conducted on materials exhibiting sigmoidal curves, using this functional form. This should be an effective way to test whether the function is suitable for inverse FEM simulation purposes. It is certainly possible that modifications to it might be needed to optimize such operations.

Acknowledgements

Relevant support was received from EPSRC (grant EP/I038691/1) and from the Leverhulme Trust, in the form of an International Network grant (IN-2016-004) and an Emeritus Fellowship (EM/2019-038/4).

Conflict of Interest

The authors declare no conflict of interest.

Data Availability Statement

Research data are not shared.

Keywords

constitutive laws, indentation plastometry, metal plasticity, sigmoidal curves

Received: June 14, 2021
Revised: September 1, 2021
Published online:

[1] J. H. Hollomon, *Trans. Am. Inst. Min. Metall. Eng* **1945**, *162*, 268.
[2] E. Voce, *J. Inst. Met.* **1948**, *74*, 537.
[3] T. W. Clyne, J. E. Campbell, *Testing of the Plastic Deformation of Metals*, Cambridge University Press, Cambridge, UK **2021**.
[4] I. Arrayago, E. Real, L. Gardner, *Mater. Des.* **2015**, *87*, 540.
[5] Y. C. Zhang, M. C. Li, H. Y. Bi, J. Q. Gu, D. X. Chen, E. Chang, W. Zhang, *Mater. Sci. Eng. A-Struct. Mater. Properties Microstruct. Proc.* **2018**, *724*, 411.
[6] M. H. Zhang, H. Y. Chen, Y. K. Wang, S. J. Wang, R. G. Li, S. L. Li, Y. D. Wang, *J. Mater. Sci. Technol.* **2019**, *35*, 1779.
[7] T. W. Mukarati, R. J. Mostert, C. W. Siyasiya, *Mater. Sci. Eng. A* **2020**, *792*, 139741.
[8] T. Masumura, T. Tsuchiyama, *ISIJ Int.* **2021**, *61*, 617.
[9] A. Blaise, B. Bourouga, B. Abdulhay, C. Dessain, in *Proc. of the ASME 11th Biennial Conf. on Engineering Systems Design and Analysis*, ASME **2012**, Vol. *2*, pp. 741–747.
[10] D. L. Beke, L. Daroczi, C. Lexcellent, V. Mertinger, *J. Phys. IV* **2001**, *11*, 119.
[11] N. Nakada, Y. Ishibashi, T. Tsuchiyama, S. Takaki, *Acta Mater.* **2016**, *110*, 95.
[12] F. Marketz, F. D. Fischer, *Modell. Simul. Mater. Sci. Eng.* **1994**, *2*, 1017.
[13] I. Y. Pyshmintsev, A. De Meyer, B. C. De Cooman, R. A. Savray, V. P. Shveykin, M. Vermeulen, *Metall. Mater. Trans. A* **2002**, *33*, 1659.
[14] C. Heinrich, A. M. Waas, A. S. Wineman, *Solids Struct.* **2009**, *46*, 364.
[15] J. Dean, J. M. Wheeler, T. W. Clyne, *Acta Mater.* **2010**, *58*, 3613.
[16] D. K. Patel, S. R. Kalidindi, *Acta Mater.* **2016**, *112*, 295.
[17] J. Dean, T. W. Clyne, *Mech. Mater.* **2017**, *105*, 112.
[18] J. E. Campbell, R. P. Thompson, J. Dean, T. W. Clyne, *Mech. Mater.* **2018**, *124*, 118.
[19] L. Meng, P. Breitkopf, B. Raghavan, G. Mauvoisin, O. Bartier, X. Hernot, *Int. J. Mater. Forming* **2019**, *12*, 587.
[20] J. E. Campbell, R. P. Thompson, J. Dean, T. W. Clyne, *Acta Mater.* **2019**, *168*, 87.
[21] T. W. Clyne, J. E. Campbell, M. Burley, J. Dean, *Adv. Eng. Mats.* **2021**, *23*, 21004037.
[22] J. E. Campbell, H. Zhang, M. Burley, M. Gee, A. T. Fry, J. Dean, T. W. Clyne, *Adv. Eng. Mats.* **2021**, *23*, 2001496.
[23] J. E. Campbell, T. Kalfhaus, R. Vassen, R. P. Thompson, J. Dean, T. W. Clyne, *Acta Mater.* **2018**, *154*, 237.
[24] Y. T. Tang, J. E. Campbell, M. Burley, J. Dean, R. C. Reed, T. W. Clyne, *Materialia* **2021**, *15*, 101017.
[25] M. Burley, J. E. Campbell, R. Reiff-Musgrove, J. Dean, T. W. Clyne, *Adv. Eng. Mats.* **2021**, *23*, 2001478.
[26] T. W. Mukarati, R. J. Mostert, C. W. Siyasiya, in *Conf. of the South African Advanced Materials Initiative*, IOP Publishing Ltd, Bristol **2019**.
[27] J. A. Nelder, R. Mead, *Comput. J.* **1965**, *7*, 308.